Reprint

Haneberg, W.C., Creighton, A.L., Medley, E.W., and Jonas, D.A., 2005, Use of LiDAR to assess slope hazards at the Lihir gold mine, Papua New Guinea, *in* O. Hungr, R. Fell, R. Couture, and E. Eberhardt, editors, *Landslide Risk Management*: Proceedings of International Conference on Landslide Risk Management, Vancouver, Canada, 31 May - 3 June, 2005, Supplementary CD.

This version contains color figures that were omitted on the conference proceedings CD.

Use of LiDAR to assess slope hazards at the Lihir gold mine, Papua New Guinea

William C. Haneberg[1]
Haneberg Geoscience, 10208 39th Avenue SW, Seattle WA 98146, USA, bill@haneberg.com

Ashley L. Creighton
Lihir Management Company, Ltd., P.O. Box 789, Port Moresby, Papua New Guinea, ashley.creighton@riotinto.com

Edmund W. Medley[1]
Medley GeoConsultants, 1554 Winding Way, Belmont CA 94002,USA, emedley@bimrocks.com

David A. Jonas
AAMHatch Pty. Ltd., 16 Julia Street, Fortitude Valley, 4006 Queensland, Australia, D.Jonas@aamhatch.com.au

ABSTRACT: The Lihir gold mine, located in Papua New Guinea, produces approximately 700,000 ounces of gold per year. It is situated within a 16 km^2 inactive and collapsed volcanic caldera with steep and inward-sloping topography, hydrothermally altered rocks, complicated geologic structures, and an active geothermal system. Precipitation averages 3.8 m/year. Dense tropical vegetation rules out traditional engineering geologic mapping as a tool for slope hazard assessment around the expanding pit, making it difficult to incorporate information from geotechnical borings into a caldera-scale geological framework. Light detection and ranging (LiDAR), also known as airborne laser scanning or airborne laser altimetry, was used to produce a digital elevation model (DEM) suitable for engineering geologic and geomorphologic interpretation. In order to ensure adequate coverage, each part of the project area was covered at least three times with a fixed-wing aircraft carrying an airborne laser scanner, yielding an average laser strike spacing of 0.4 m. The LiDAR returns were dense enough to interpolate a 2 m gridded DEM beneath the vegetation, which was in turn used to produce a series of geomorphologic maps that were analyzed in a GIS framework. Two- and three-dimensional shaded relief images with varying angles of illumination allowed identification of naturally occurring and human-induced landslides, debris fan complexes, caldera-scale rock slumps, lineaments, and young fault scarps. Topographic roughness, defined as the standard deviation of residual topography within a moving window, was especially useful for distinguishing colluvium landslides from rock slumps and intact rock as well as identifying individual lobes of a debris fan. The potential for shallow landslides and debris flows was also evaluated by classifying slope angle and plan curvature at each raster according to the SMORPH algorithm. Field verification showed the LiDAR DEM to be a faithful representation of topography around the mine and an invaluable tool for hazard assessment.

1 INTRODUCTION

Located on Lihir Island in the New Ireland province of Papua New Guinea, the Lihir mine is one of the world's largest gold mining and processing operations. The epithermal sulfide gold deposit was discovered in 1983 and mining commenced in 1997. Mining is scheduled to continue until 2023, after which stockpiled ore will be processed until 2040. Gold occurs in three distinct structurally controlled ore bodies (named Minifie, Lienetz and Kapit) and reserves have increased during mine development, from 454,000 kg (14.6 million ounces) in 1996 to 634,400 kg (20.4 million ounces) with an average ore grade of 3.88 grams per metric tonne in 2003. Out-of-pit material movements between 1998 and 2004 ranged between 27.9 and 46.8 million metric tonnes.

[1] Consultant to Condor Earth Technologies, Sonora, California, USA.

The three deposits will be mined using separate but adjacent pits. Excavation of the Minife pit, which began in 1997, is nearly complete. Stripping for the Lienetz pit began in 2003 and mining is expected to begin in 2005. Excavation of the Kapit pit has not yet started. Current and anticipated geotechnical challenges within the Lienetz pit include weak hydrothermally altered rock and an active geothermal system that produces high rock temperatures and fluid pressures.

In addition to the usual difficulty of excavating large pits in weak rock, site conditions pose unique geotechnical challenges as the pits expand into inward sloping and tropically weathered surficial deposits within the bowl-shaped caldera. Locations must also be found for large stockpiles of low-grade ore that will remain in place until the ore is processed between 2023 and 2040. Although the mine conducts an active geotechnical exploration programme, the dense jungle canopy makes it virtually impossible to perform engineering geologic mapping or aerial photographic interpretation in order to provide a framework to help interpret existing geotechnical data and plan future drilling.

In order to better assess the potential for geotechnical problems posed by pit expansion and stockpile placement in increasingly steep and vegetated terrain, Lihir Management Company contracted with AAM Hatch to collect and process airborne LiDAR elevation coverage of the mine and surrounding areas. Condor Earth Technologies was retained to produce a LiDAR-based DEM suitable for geologic interpretation, perform a terrain hazard assessment, and conduct limited field verification at the mine site. The LiDAR data were collected and processed in August 2004. Geological data processing and interpretation occurred in early September 2004, followed by limited field verification and minor map revisions in late September.

2 GEOLOGIC SETTING

2.1 *Location and Regional Tectonics*

The Lihir gold mine is on Lihir Island, New Ireland, Papua New Guinea. The island is, in turn, located at 3° S latitude and 153° E longitude, about 980 km NE of Port Moresby, the national capital (Fig. 1). Lihir is part of the Tabar-Lihir-Tanga-Feni chain of volcanic island groups between and parallel to New Ireland and the inactive (6000 m deep) Kilinailau trough. Each island group is on a N to ENE trending submarine ridge developed along back arc transfer faults oblique to the coast of New Ireland (Hunt, 2002).

2.2 *Lihir Island Geology and Volcanology*

Lihir is a 20 km by 13 km volcanic island formed from three Pliocene-Pleistocene volcanoes (Huniho, Kinami, and Luise) superimposed on a basement of Late Miocene stratovolcanoes that arose in 2000 m deep water (Hunt, 2002). The open pit Lihir gold mine, the subject of this paper, is located within the Ladolam gold deposit at the floor of the 1 My old Luise caldera (Letten and Hunt, 2000; Hunt, 2002). The caldera collapsed seawards towards the northeast, creating Luise Harbor and a submarine debris fan extending 10 km from the island (Hunt, 2002). In map view, the remains of the collapsed caldera form an ellipse approximately 6 km by 4 km, with the pre-mining crater floor (southwest) having an undulating topography to 130 m above sea level. The floor is bounded by very steep and fluted walls as high as 600 to 700 m above the caldera floor. The pre-collapse volcano may have been as high as 1400 m (Letten and Hunt, 2000).

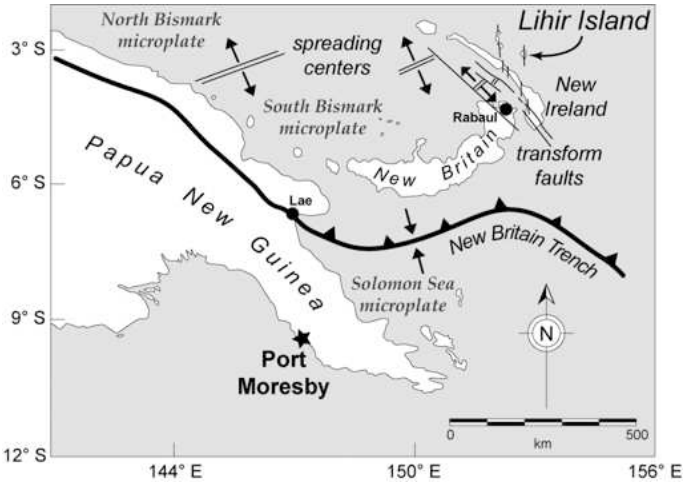

Figure 1. Index map showing the location of Lihir Island in relation to Port Moresby and major tectonic features. The Kilinailau trough is north of the map area. Modified from Letten and Hunt (2000).

The volcanic edifice of Lihir is composed of alkali basalt flows with abundant pyroclastic breccias and tuffs. Alkaline monzonite stocks moved into the base of Luise volcano, at least up to sea level, between 0.9 and 0.4 My ago. The resulting porphyry stage resulted in extensive alteration within the original volcano, pressure-induced weakening of the 1200 m high edifice, and eventual caldera collapse about 0.35 My ago.

Collapse of the volcanic edifice likely occurred as sideways unroofing (Corbett & Leach, 1998, p. 142) in which a considerable proportion of the volcano was removed in one or more catastrophic slope failures. Recent literature (Day, 1996; Voight & Elsworth, 1996) suggests that such catastrophic volcanic collapses (e.g. in 1980 at Mt. St. Helens, Washington, USA) are due to pressure increases

within volcanoes because of magma intrusions and rejuvenation of volcanism, typically accompanied by increased groundwater pressure, seismic loading, and reduction of rock mass permeability as rock caps are converted to clays by hydrothermal alterations. At the Luise caldera, unloading resulted in intrusion and quenching by seawater, extensive normal listric faulting, large-scale magmatic-hydrothermal and phreato-magmatic explosive breccias and diatreme breccias, pervasive alteration of rock, and precipitation of structurally-controlled mineral deposits (Letten and Hunt, 2000). This complicated geological history of multiple deformation episodes and pervasive alteration makes it difficult to distinguish among the breccias (Hunt, 2002).

2.3 *Current Conditions*

Current geological conditions within the caldera include an active geothermal regime with temperatures exceeding 100°C near the ground surface in some places, a complicated and poorly understood network of faults and joints (including major listric normal faults that control ore grade and location), and deeply weathered and hydrothermally altered rock and tropical soils. Back-calculated angles of internal friction for clayey soils involved in previous landslides are as low as 7° and pore water pressures are locally high. Slopes surrounding the pits mine are covered with dense jungle (Figs. 2-3), making detailed engineering geologic mapping or aerial photo interpretation virtually impossible. These factors combine to produce unique mining engineering, geotechnical engineering, and engineering geological challenges.

Figure 2. View of dense jungle cover from ground level, with the caldera rim in the background.

The climate at Lihir is equatorial, with annual average rainfall of 3.8 m and individual storms of torrential intensity. Air temperatures range from 19°C to 35°C.

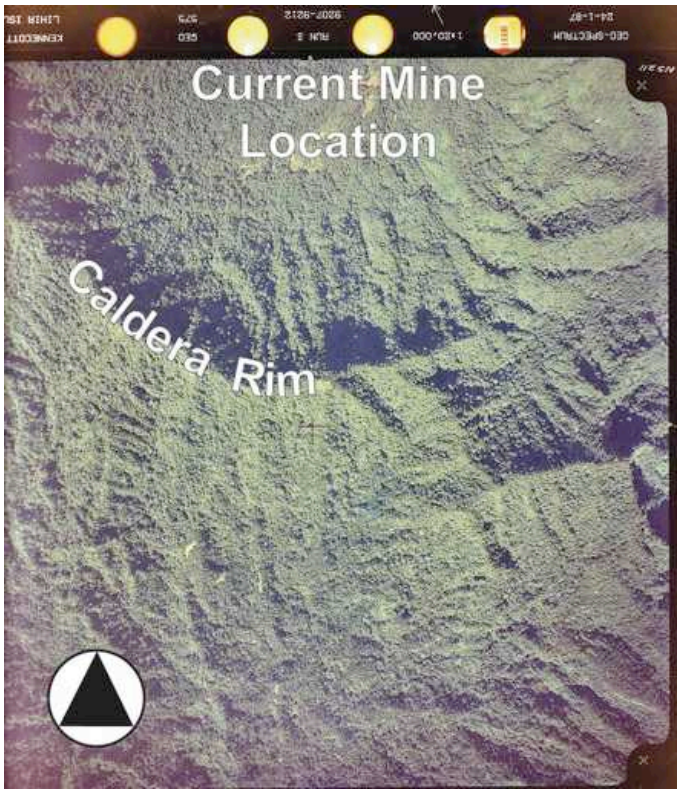

Figure 3. Pre-mine aerial photograph showing dense jungle covering undeveloped portions of the project area. The Lihir mine is located within the curved caldera in the upper 1/3 of the photograph. Relief between the caldera floor (mine site) and rim is approximately 875 m.

3 LIDAR DATA COLLECTION

LiDAR has been commercially available since 1994. Although its implementation is complicated, the basic idea behind LiDAR is simple, involving three measuring devices fitted to a fixed-wing aircraft or helicopter. The three devices are:

1 A survey-grade GPS receiver to record the position of the aircraft every 0.5 second.

2 A high-accuracy Inertial Reference System (IRS) records the roll, pitch and heading (orientation) of the aircraft, at a rate of 200 times per second.

3 A pulse laser that emits a discrete laser beam, which is reflected from the terrain below. Distance between the aircraft and ground is calculated from the laser travel time.

Data from the three instruments are combined to compute the 3D coordinates of the features from which the laser has reflected. Laser measurement rates depend upon the LiDAR equipment. The instrument used for this project measured 25,000 points every second (25 kHz). At this rate, the unit measured an array of spot heights 1.4m apart. A major part of the LiDAR data processing involves assessing the computed *x-y-z* coordinates to ascertain

what the laser has reflected off. One needs to remove all non-ground LiDAR strikes if a bare earth model or digital elevation model (DEM) is the desired end product.

Because no suitable aircraft were available locally, the equipment for this project was flown from Australia to Lihir Island in a fixed-wing aerial survey aircraft. Once on the island, flight planning was complicated by local conditions. Flying at 1100 m above the ground, the aircraft had to contend with 875 m relief between the bottom and the top of the caldera. This represented a large percentage of the nominated flying height, which posed a navigation challenge and safety hazard. Weather presented another challenge, because the laser does not penetrate clouds. The caldera rim is persistently shrouded in clouds, rainstorms occur almost daily, and steam from geothermal pressure relief wells creates localized plumes (Fig. 4). The final challenge to flight planning was the GPS satellite constellation. GPS positioning relies on 24 satellites, but the number of satellites overhead can vary throughout the day. LiDAR flight planning must therefore take into account satellite availability in order to avoid times when fewer than six satellites are visible from the study area. Data collection sorties were attempted from 3:00 a.m. to late evening, resulting in six hours of data collection over a five-day period. Each part of the project area was covered at least three times. In all, 9,656,000 ground strikes and 86,237,000 non-ground strikes were recorded.

Preliminary data processing was completed on-site in order to locate gaps in coverage caused by cloud shadows or terrain variations, and six extra sorties were flown to eliminate gaps. Preliminary on-site data processing was a vital step to ensure adequate coverage before the aircraft and flight crew were demobilized from this remote site. Subsequent office data processing included editing of the data to remove non-ground LiDAR strikes and conversion of the data from WGS84 to Lihir mine grid coordinates using a seven-parameter Helmert transformation tied to nine ground reference points.

Jungle canopy penetration was as low as 5% of the total emitted points in some parts of the project area. This meant that, although the LiDAR was sampling the canopy every 0.4m, laser strikes defining the ground were as much as 10 m to 20m apart in the most densely covered areas. This density was sufficient, however, to clearly delineate the drainage patterns and geomorphology in the covered areas around the active pits.

4 DIGITAL ELEVATION MODEL

The digital elevation model (DEM) used for this project was generated by using inverse squared distance interpolation to create a regular grid of 9,578,830 points (3830 E-W rows and 2501 N-S columns) from *x-y-z* data points supplied by AAM Hatch. Of those points, 6,567,670 contained elevation values and the remainder were void or no-value points outside of the irregularly shaped study area (Fig. 5). The DEM grid spacing of 2 m was chosen by plotting the LiDAR bare earth return data and examining it to ensure that grid cells containing elevation data were separated from each other by no more than 4 or 5 empty cells in heavily vegetated areas adjacent to the pit. This is an important consideration because selection of an inappropriate interpolation method and/or grid spacing can give rise to interpolation artifacts that obscure subtle geologic features and make interpretation difficult. It would have been possible to generate a much more closely spaced DEM grid in open areas, but the results would have been unacceptable for the vegetated terrain that was the focus of our hazard assessment.

Figure 4. Persistent cloud cover and steam plumes rising from geothermal pressure relief wells posed a problem for LiDAR data collection. The large barren earthwork in the middle ground is an ore stockpile, and the dark area in the distance is dense jungle cover.

5 GEOMORPHIC DERIVATIVE MAPS

The second step of the assessment was to use the 2 m DEM as the basis for a series of geomorphic derivative maps. As explained in Section 5, the geomorphic maps were intermediate products used to produce interpretive hazard maps. Except where specified otherwise, these maps were produced using the commercial raster GIS software MFworks 3.0. Space limitations allow inclusion of only a few of the geomorphic derivative maps.

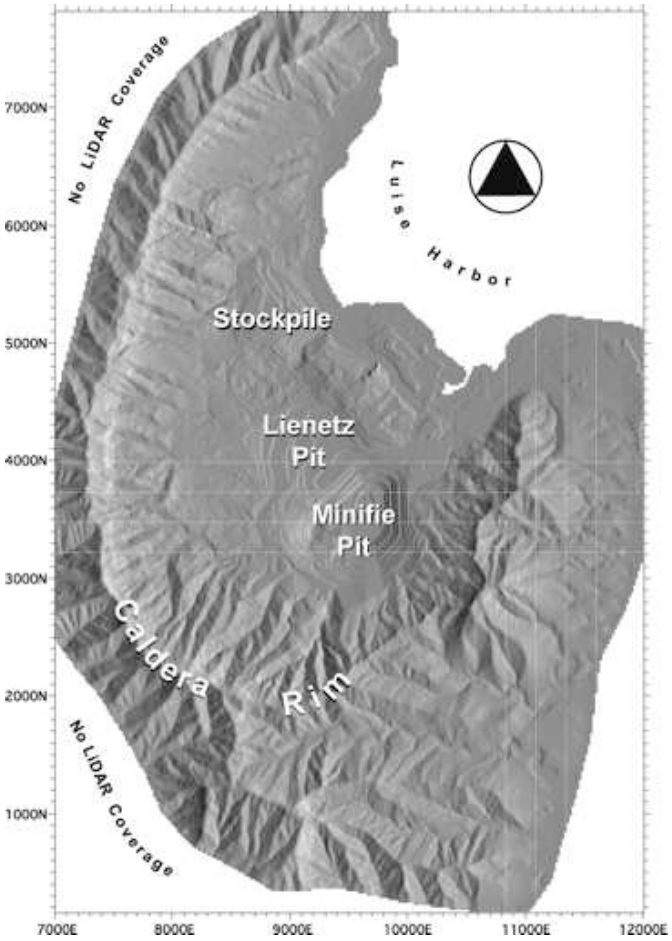

Figure 5. Shaded relief map produced from the Lihir mine 2 m DEM, with illumination from the east. Labeled stockpile is the same as shown in Figure 4. Major ticks are 1000 m intervals in the Lihir mine grid, minor ticks are 100 m. North is to the top.

5.1 *Shaded Relief*

Five shaded relief maps were created by convolving simple 3 by 3 kernels with the DEM in order to simulate illumination from the west, northwest, north, northeast, and east. One shaded relief map is shown in Figure 5. Illumination from the south was avoided because it creates the optical illusion of inverted topography. Shaded relief maps with different sun angles are useful for identifying topographic features and lineaments oriented at high angles to the illumination. Figure 5 shows that, even when reduced to column width, the shaded relief maps include a considerable amount of geomorphic detail. The shaded relief maps were also a useful navigation aid during the field verification portion of this project.

5.2 *Topographic Contours*

A raster contour map was created by slicing the DEM at 10 m intervals, filtering, and recoding the resulting values. It was used for geomorphic interpretation in conjunction with the shaded relief, slope angle, and topographic curvature maps described below.

5.3 *Smoothed Topography*

A smoothed version of the DEM was created by averaging elevation values within a 5-cell moving window. This map was an intermediate product necessary to calculate residual topography and topographic roughness maps and was not used directly for geomorphic interpretation.

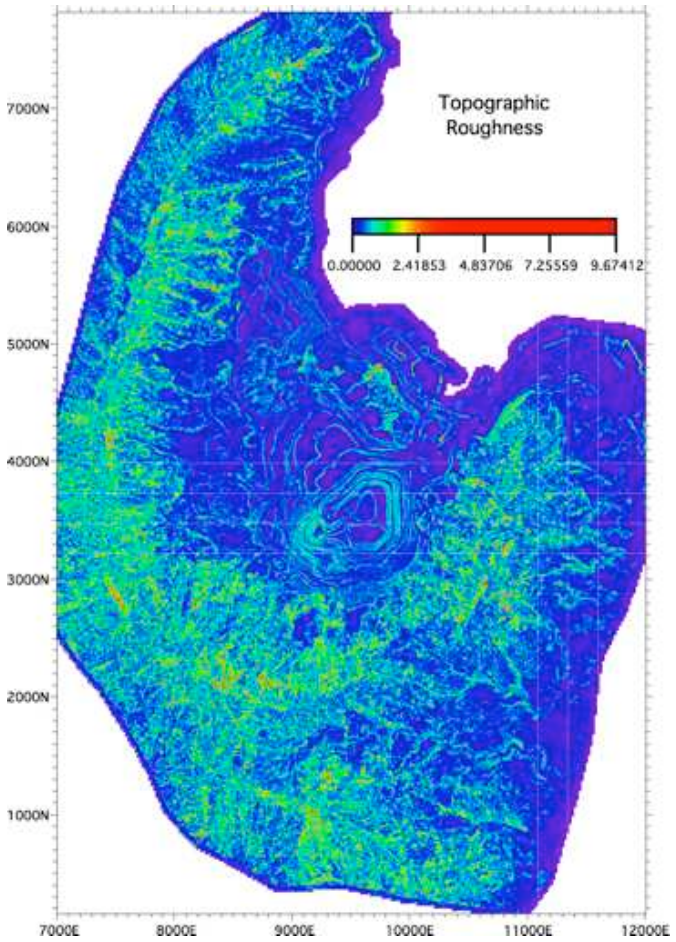

Figure 6. Topographic roughness map with units of ±metres. Lihir mine grid coordinates in metres.

5.4 *Topographic Roughness*

Topographic roughness maps (Fig. 6) can aid in terrain classification and, of particular relevance to this project, landslide delineation by emphasizing differences in surface texture among different surficial

deposits and landforms (Barnett et al., 2004, McKean & Roering, 2004). In this project, roughness is defined as the standard deviation of residual topography within a circular moving window of specified size (in this case 5 cells). As such, it has units of ±meters. This approach has at least four advantages over other methods. First, it is easy to implement using raster GIS map algebra because it does not use eigenvalues or Fourier spectra. Second, unlike eigenvalue techniques, it does not have the potential to produce erroneously high roughness values in flat areas with large raster-to-raster variations in slope aspect. Third, the use of residual topography helps to filter out the effect of large-scale topography and facilitate identification of features at the scale of the moving window. Fourth, this method generally produces more sharply defined results than a Laplacian filter (which is also easy to apply in a raster GIS).

Roughness values ranged from zero to ±9.7 m, although almost all of the values were less than ±2.4 m (Fig. 6). Of particular interest is a large and relatively smooth area just to the west of the pits and a number of smaller fingers of relatively smooth terrain. The significance of these anomalies will be discussed in Section 6.3.

5.5 *Slope Angle and Slope Angle Class*

The slope angle at each grid point was calculated by taking the largest of 4 slope angles calculated using a finite difference operator applied to pairs of the surrounding 8 grid points. The slope angle map was found to be a useful tool for delineating geomorphic units when combined with the shaded relief, contour, and topographic roughness maps. A slope angle class map, required for the SMORPH hazard map described in section 6, was created using an 11-cell moving window average to smooth the slope angle map and then dividing the result into 5 classes. Figure 7 shows the maximum slope angle map, with slope angles ranging from horizontal along benches and the pit floors to nearly vertical along the edge of the caldera rim.

5.6 *Plan Curvature and Plan Curvature Class*

Plan curvature, which is the curvature of contour lines in map view, was calculated using an 11-cell moving window. The curvature calculations were performed by LandSerf 2.1, a freely available digital terrain analysis programme, and imported into MFWorks 3.0 for additional manipulation. A plan curvature class map, required for the SMORPH analysis described in section 6, was created by classifying grid points with curvature ≤ 0.01 m^{-1} as convex, those with plan curvature ≥ 0.01 m^{-1} as concave, and those in between as planar.

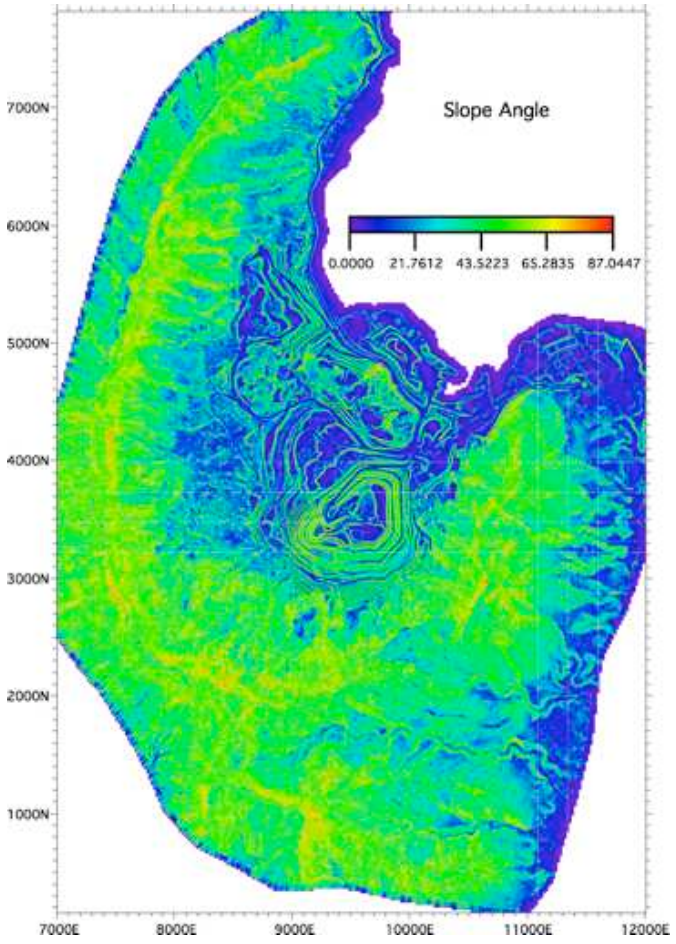

Figure 7. Maximum slope angle map, in degrees. Lihir mine grid coordinates in meters.

5.7 *Ridge and Channel*

The ridge and channel map is a variation of the plan curvature class map in which the planar class boundaries are widened to ±1 m^{-1}. This accentuates narrow zones of highly convex and concave topography that comprise ridges and channels. This map was used to evaluate the geometry and maturity of drainage systems developed in different bedrock or geomorphic map units in the project area.

6 INTERPRETIVE MAPS

The geomorphic derivative maps described in Section 5 were used as the basis for three interpretive maps useful for hazard and risk assessment.

6.1 *SMORPH Shallow Landslide Hazard Map*

SMORPH, an acronym for Slope MORPHology, is a semi-empirical method developed by the Washington (USA) Department of Natural Resources to identify portions of steep watersheds susceptible to shallow landslides that can mobilize into debris flows. The method is computationally simple and therefore

well suited to raster GIS implementation. More importantly, SMORPH can produce results that are as good as, if not better than, computationally intensive algorithms that incorporate steady-state groundwater flow models (Shaw & Vaugeois, 1999).

Each SMORPH map grid point receives a low, medium, or high hazard rating based on the slope angle class and plan curvature class maps (Table 1). The slope angle class and plan curvature class maps calculated using 11-cell moving windows were used because smaller 3- and 5-cell windows produced maps with discontinuous channel segments.

	Plan Curvature Class		
Slope Angle	Convex	Planar	Concave
$0° \le \theta < 6°$	*Low*	*Low*	*Low*
$6° \le \theta < 12°$	*Low*	*Low*	*Medium*
$12° \le \theta < 18°$	*Low*	*Low*	*High*
$18° \le \theta < 25°$	*Low*	*Medium*	*High*
$\theta \ge 25°$	*Medium*	*High*	*High*

Table 1. SMORPH landslide hazard matrix for the Lihir mine project. Hazard ratings are assigned using plan curvature class and slope angle class maps as described in Section 5.2.

SMORPH slope angle class boundaries can be derived from landslide inventories of geologically similar terrain or limit equilibrium slope stability analyses. In this case, no inventory maps existed. The uppermost slope category of $\theta > 25°$ was chosen because 25° is the steepest slope upon which a thin uniform layer of frictional soil with a typical angle of internal friction of $\phi = 25°$ will be stable under dry conditions (*i.e.* an infinite slope calculation). Steeper slopes will be unconditionally unstable with respect to shallow landslides, and the stability slopes with $12° \ge \theta > 25°$ will depend on pore water pressure. Planar slopes less than 12° should be unconditionally stable under our assumptions. The remaining two boundaries were obtained by halving the 12° and 25° boundaries. The threshold value of $\phi = 25°$ is a somewhat conservative first estimate adequate for reconnaissance purposes, and which can be refined (or augmented with cohesive strength) as additional site-specific geotechnical data become available.

The Lihir mine SMORPH map (Fig. 8) classifies most of the steep slopes surrounding the mine as medium to high hazard terrain, depending on curvature, with respect to shallow landslides. A notable exception is the area just west of the active mine operations (8000 to 9000 E, 3000 to 5000 N), which is characterized by high and low hazard terrain with essentially no medium hazard ground. Comparison of the SMORPH map with the slope angle map (Fig. 7) and topographic roughness map (Fig. 6) shows that this anomalous area is also characterized by lower slope angles and relatively smooth topography. The interpretation of this relationship is discussed in Section 6.3.

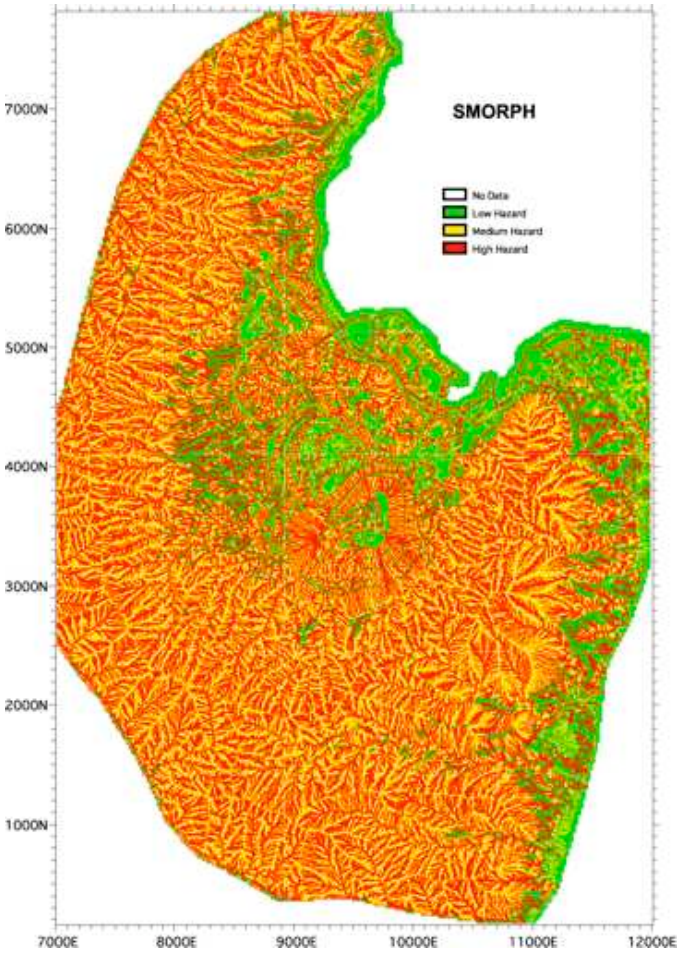

Figure 8. SMORPH shallow landslide hazard map.

Other anomalously low hazard areas on the SMORPH map (e.g. 8000 to 9000 E, 5000 to 6000 N and 9000 to 9500 E, 3800 to 4400 N) consist of ground occupied by ore stockpiles or active portions of the mine with flat graded surfaces.

6.2 *Lineament Map*

The lineament map, shown together with a shaded relief image, the terrain hazard map, and a geologic map in Figure 9, depicts linear features visible on the shaded relief images without regard to origin or geologic significance. The lineament map was created by identifying features on each of the five shaded relief images, and then combining the results into one map layer.

6.3 *Terrain Hazard Map*

The terrain hazard map is a qualitative product based on objective information (*e.g.* slope angle and topog-

raphic roughness) supplemented by qualitative field and office observations, professional judgment, and experience. It does not include information about the relative stability of slope hazards and, as such, is analogous to the engineering geologic map (middle) layer in the three-tiered hazard mapping system used by Haneberg et al. (2002). The utility of the terrain hazard map depends on the ability of an experienced geologist to interpret landforms and terrain anomalies, compare and contrast them to similar patterns observed elsewhere, and draw inferences based upon the available information.

The terrain hazard map was prepared in the office by overlaying various combinations of the derivative maps described in Section 5, with the objective of identifying geomorphic anomalies or patterns that might be indicative of underlying terrain hazards. In doing so, an iterative procedure was followed that maximized the utility of information contained in the DEM. The order of the layers could be changed and their transparencies adjusted individually in order to help delineate map units that are distinct in both their geomorphologic signatures and hazard implications. Terrain hazard map unit boundaries were drawn as vector artwork in a separate layer that could be edited without changing the underlying layers. Then, the results were draped over the DEM to create 3D renderings of the area that could be examined on a large high-resolution computer monitor at different view angles and modified as necessary (Fig. 10). This process was repeated until a draft terrain hazard map suitable for field verification was created.

The following units comprise the terrain hazard map units shown in Figure 9:

6.3.1 *Rockslides or rockslumps*

These are potentially deep-seated features that may have been related to caldera collapse and which appear to be rotated along listric slip surfaces. In the case of the rockslide/rockslump complex near the southwestern portion of the pit, a pronounced and highly incised topographic irregularity extends farther into the caldera than adjacent slopes. Another occurrence of this unit at approximately 3700N-8000E is shown as an intrusive dyke on the island geologic map (Fig. 9), probably on the basis of premining aerial photograph interpretation. No signs of intrusive rock outcrops or float were found during our field reconnaissance and this feature is interpreted as a back-rotated rock slump block by virtue of its shape and location relatively high on the caldera wall. Toes of the rockslide/rockslumps appear to be covered by accumulations of talus and/or colluvium, including smaller colluvium landslides in valleys. LiDAR strikes in this map unit are more patchy and concentrated in small zones, which may reflect the presence of rock or domains of vegetation, stunted because of rock near the surface.

The large southwestern rockslide does not appear to be associated with an alteration zone, at least as shown on the island-scale geologic map, but may be associated with local or regional geologic structures. Limited field observations also indicated relatively unaltered volcanic rock with still-distinct amygdules in some parts of this map unit. Experience suggests that internal stratigraphy can remain nearly intact within the rotated blocks. These features may, therefore, be interpreted by some geologists as fault blocks.

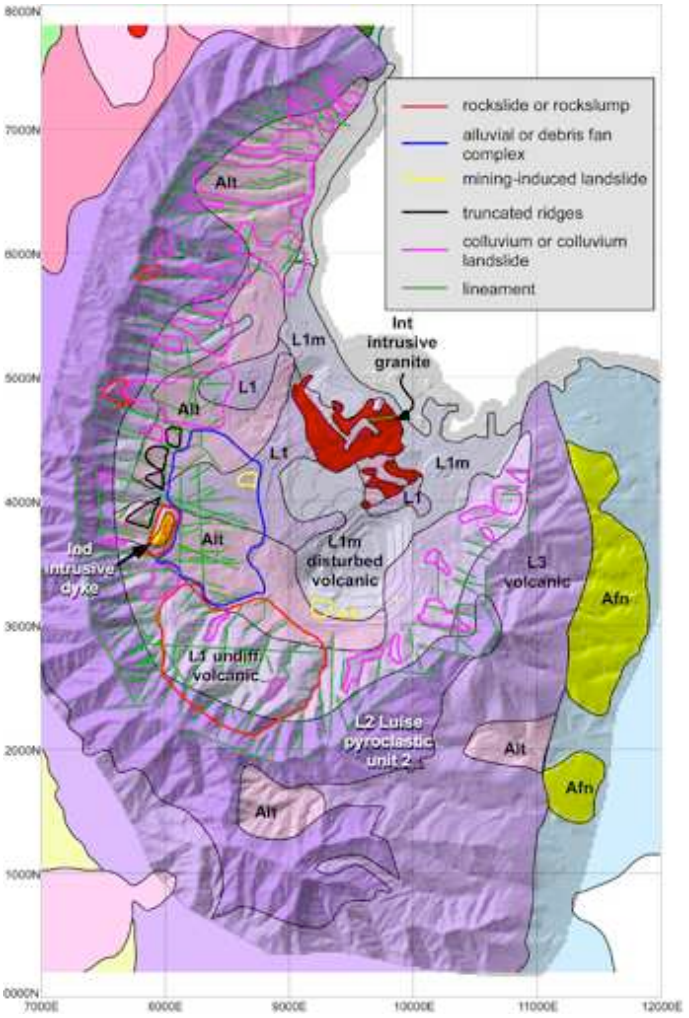

Figure 9. Terrain hazard, lineament, and geologic maps superimposed on a shaded relief image of the project area. Terrain hazard mapping was restricted to the area within the caldera rim and did not include areas inside of the active pits. Geologic map is from Lihir Management Company files. Afn: alluvial fan, Alt: hydrothermally altered volcanic rocks, Int: intrusive granite, Ind: intrusive dyke, L1, L2, L3: volcanic and pyroclastic units of Luise caldera

6.3.2 *Mining-induced landslides*

These features are associated with ongoing mining, and were identified on the basis of characteristic landslide morphology, sharp boundaries, and proximity to mining activities. Mining induced landslides occur in both intact (but altered and/or weathered) volcanic rock, residual soils developed on the volcanic rocks, and transported soils delivered by surface water flow, debris flows, or rockfall.

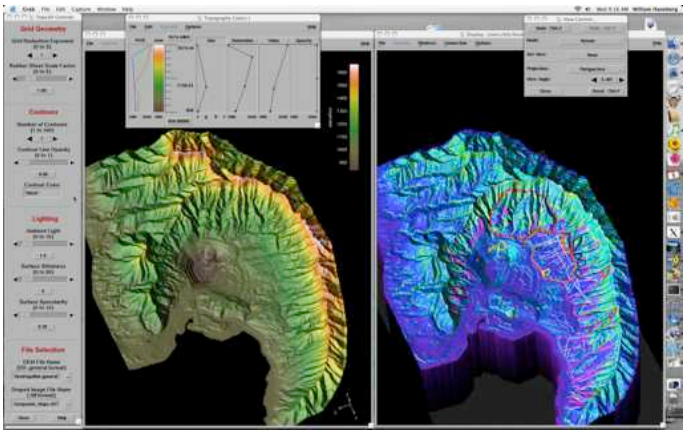

Figure 10. Screen capture of a computer program developed in-house for terrain visualization and interpretation of high-resolution LiDAR DEMs. The left pane shows the LiDAR DEM colored according to elevation. Contour lines can be added but are not shown here. The right pane shows the topographic roughness, lineament, terrain hazard maps draped over the DEM (note that map unit colors are different than in Figure 9). Zoom and rotation controls operate on both panes simultaneously, allowing the analyst to compare two or more data layers and refine map units by examining the geomorphology from different angles and with different lighting conditions.

6.3.3 *Truncated ridges*

Several ridges west of the mine are truncated by steep and planar facets suggestive of past faulting or landslide movement. They may be the head scarps of large caldera collapse rockslides similar to those described in Section 6.3.1, although there are no well-defined landslide or rockslide blocks adjacent to the facets.

6.3.4 *Alluvial or debris fan complexes*

This unit consists of coalescing and moderately well channelized alluvial and debris fans characterized by relatively low slopes, hummocky but smooth topography, and short disconnected channel segments. General knowledge suggests that the internal stratigraphy most likely consists of stacked buried soils, debris flow deposits, alluvium, and colluvium that grades into landslides. Small-scale depositional units, for example individual channel deposits, are likely to be relatively discontinuous, with much more radial than tangential continuity, making detailed subsurface characterization (particularly using arbitrarily located boreholes or gridded drilling programs) and slope stability analysis difficult. Clayey buried soils and faults such as those interpreted from the lineament map may serve as localized aquitards responsible for artesian pore water pressures that have been observed during geotechnical drilling. Moreover, tropical weathering of volcanic rocks to clays with very low angles of internal friction (potentially in the range of $5° \leq \phi \leq 10°$) have created the potential for movement along very gently dipping slip surfaces. This map unit corresponds largely to the active alluvial fans described in the SMORPH map section, so flooding and debris flow delivery present additional hazards.

Overlays of the shaded relief, contour, and roughness maps show that this unit is actually composed of at least three sub-units: two alluvial fans separated by a zone of slightly rougher topography, and a debris field that appears to originate from a North-striking elliptical rock slump block centered at about 3700N and 8000E in Figure 9. The difference in surface roughness might reflect differences in the ages of the geomorphic surfaces or differences in parent material size (note the correspondence between the hydrothermally altered geologic map unit Alt in Figure 9 with an area of slightly increased roughness in Figure 6).

Field observations suggest that the alluvial and debris fan complex is generally unstable, and that slope failures have been common and recent. Deposits comprising this map unit are cut by many fresh scarps and have a step-like topography consistent with recent or current landsliding. Likewise, the existence of many short channel segments, lack of a well-established drainage network, and springs at between approximately 1050m and 1070 m elevation all suggest that the slope has been recently active. Streams incised 10 m or more below adjacent terraces and boulders of 1 m or more in diameter were also observed suggesting that, although debris flows do not currently reach the active pit area, they may become a hazard as pit expansion moves toward the caldera walls.

6.3.5 *Colluvium and colluvium landslides*

These features were identified by their topographic smoothness, moderate to relatively steep slopes, elongate form, lobate toes, and absence of fan-like distributary channel systems. Not every mapped occurrence exhibits all of these properties and, moreover, it is not possible to discriminate between slowly creeping and more rapidly sliding colluvium solely on the basis of geomorphic analysis. It is also possible that a slope can alternate between the two modes of movement as pore water pressure changes, for example during unusually prolonged or intense storms, or as the result of seismic shaking, logging, or cutting and filling. The thickness of these units is likely

to range from many meters to tens of meters. They pose a hazard because, even if currently stable, movement may be triggered by placement of fill or cutting through the toes.

7 RISK ANALYSIS

The reconnaissance nature of this project made it impossible to quantitatively assess the risks posed by terrain hazards that were identified around the mine. Risks for each of the map units were, however, qualitatively assessed by considering the likelihood of occurrence (e.g. certain, likely, unlikely) over the remaining life of the mine and the possible consequences of occurrence (e.g. injury or loss of life, damage to equipment or infrastructure, inability to recover ore). The results of this work will help to define future geotechnical exploration targets and allocate geotechnical resources, and provide a caldera-wide framework in which existing and future geotechnical information can be interpreted.

8 SUMMARY

A high-resolution LiDAR DEM allowed an efficient reconnaissance level terrain hazard assessment to be conducted in the area surrounding the remote Lihir gold mine, where a dense jungle makes traditional engineering geologic mapping and aerial photograph interpretation virtually impossible. Multiple passes and on-site preliminary LiDAR data processing allowed gaps in the coverage to be filled and a useful DEM to be produced in spite of unfavorable atmospheric conditions and heavy ground cover. Creation of a DEM with appropriate grid spacing in geologically critical areas helped to minimize interpolation artifacts that can make geologic interpretation difficult. The use of several kinds of derivative geomorphic maps, shaded relief maps, and interactive computer map layering and rendering of 3-D surfaces allowed identification of subtle differences in topography. This allowed potential terrain hazards to be mapped in the office before traveling to the mine for limited field verification.

In general, little relationship was found between bedrock geologic units shown on a previously existing map and the terrain hazard units. In some cases, features that were identified as landslides or other unstable features corresponded to areas mapped as hydrothermally altered rock, but in other cases they did not. In one case a feature mapped as a dyke appears more likely to be a back-rotated rockslump block.

The LiDAR elevation data have proven useful in other aspects of mine operations. Estimates of overburden stripping volumes were reduced when recalculated using a LiDAR DEM. High resolution topographic maps have also proven useful for surface water hydrology and environmental projects at the mine. Based on the experience gained in this study, it is believed that high-resolution LiDAR DEMs can be extremely effective tools for site selection, transportation corridor planning, and mineral exploration in areas covered by dense jungles.

9 ACKNOWLEDGEMENTS

Haneberg and Medley are grateful for the administrative support and technical review provided by Condor Earth Technologies, particularly Dr. Barry Hillman and Dr. Ron Yeung. We also benefited from discussions with Paul Maconochie of GeoTec Solutions, and comments by Jan Anderson and Garrick Mendham of Lihir Management Company. MFworks is a trademark of Keigan Systems, Inc.

REFERENCES

Barnett, P.J., Singhroy, V.H., Shirota, J., Leney, S.J. 2004. Methods for remote engineering geology terrain analysis in boreal forest regions of Ontario, Canada. *Environmental & Engineering Geoscience* 10: 229-241.

Corbett, G. J. & Leach, T.M. 1998. Southwest Pacific rim gold-copper systems: structure. In *Alteration, and mineralization*. Littleton, Colorado: Society of Economic Geologists, Special Publication No. 6: 37-200.

Day, S.J., 1996, Hydrothermal pore fluid pressure and the stability of porous, permeable volcanoes. In W.J. McGuire, A.P. Jones, J. Neuberg (eds.), *Volcano Instability on the Earth and Other Planets*. London: Geological Society of London, Special Publication 110: 77-93.

Haneberg, W.C. 2004. *Computational Geosciences with Mathematica*. Berlin: Springer-Verlag.

Haneberg, W.C., Bauer, P.W., & Chávez, W.X., Jr. 2002. Multilevel geologic hazard assessment mapping in the Rio Grande gorge, northern New Mexico, USA. In P. T. Bobrowsky (ed.), *Geoenvironmental Mapping: Method, Theory and Practice*. Rotterdam: Balkema: 75-91.

Hunt, S.J. 2002. The discovery of structure confined blind ore extensions to the Ladolam deposits, Lihir, PNG. In *Exploration in the Shadow of the Headframe*. North Sydney: Annual Meeting of the Sydney Mineral Exploration Discussion Group, October 11, 2002. http://www.smedg.org.au/hunt02.pdf

Letten, R. & Hunt, S. J. 2000. *Presentation to Investors on Lihir Gold Mine, September 4-7, 2000*. http://www.lihir.com.pg/press/aug00/presentation2pts.zip

McKean, J. & Roering, J. 2004. Objective landslide detection and surface morphology mapping using high-resolution airborne laser altimetry. *Geomorphology* 57: 331-351.

Shaw, S.C. & Vaugeois, L.M. 1999. *Comparison of GIS-Based Models of Shallow Landsliding for Application to Watershed Management*. Olympia: Washington Department of Natural Resources Report TFW-118.

Voight, B. & Elsworth, D. 1997. Failure of volcano slopes. *Géotechnique* 47: 1-31.